Miyawaki A, Griesbeck O, Tsien RY (1999) Dynamic and quantitative Ca^{2+} measurements using improved cameleons, Proc Natl Acad Sci USA **96**: 2135-2140 PMID: 15208716

Miyawaki A, Llopis J, Heim R, McCaffery JM, Adams JA, Ikura M, Tsien RY (1997) Fluorescent indicators for Ca^{2+} based on green fluorescent proteins and calmodulin, Nature **388:** 834-835 PMID: 9278050

Miwa H, Sun J, Oldroyd GE, Downie JA (2006) Analysis of calcium spiking using a cameleon calcium sensor reveals that nodulation gene expression is regulated by calcium spike number and the developmental status of the cell. Plant J **48**: 883-94 PMID: 17227545

Nagai T, Ibata K, Park ES, Kubota M, Mikoshiba K, Miyawaki A (2002) A variant of yellow fluorescent protein with fast and efficient maturation for cell-biological applications. Nature Biotechnol **20**, 87-90 PMID: 11753368

Nagai T, Yamada S, Tominaga T, Ichikawa M, Miyawaki A (2004) Expanded dynamic range of fluorescent indicators for Ca^{2+} by circularly permuted yellow fluorescent proteins. Proc Natl Acad Sci USA **101**: 10554-10559 PMID: 15247428

Ordenes VR, Reyes FC, Wolff D, Orellana A (2002) A thapsigargin-sensitive Ca^{2+} pump is present in the pea golgi apparatus membrane. Plant Physiol **129**: 1820-1828 PMID: 12177495

Palanivelu R, Brass L, Edlund AF, Preuss D (2003) Pollen tube growth and guidance is regulated by POP2, an arabidopsis gene that controls GABA levels. Cell **114:** 47-59 PMID: 12859897

Parton RM, Fischer-Parton S, Trewavas AJ, Watahiki MK (2003) Pollen tubes exhibit regular periodic membrane trafficking events in the absence of apical extension. J Cell Sci **116**: 2707-2719 PMID: 12746485

Petersen OH, Michalak M, Verkhratsky A (2005) Calcium signaling: past, present and

future, Cell Calcium **38**: 161-169 PMID: 16076488

Pierson ES, Miller DD, Callaham DA, Shipley AM, Rivers BA, Cresti M, Hepler PK (1994) Pollen tube growth is coupled to the extracellular calcium ion flux and the intracellular calcium gradient: Effect of BAPTA-type buffers and hypertonic media. Plant Cell **6**: 1815-1828 PMID: 7866026

Pierson ES, Miller DD, Callaham DA, van Aken J, Hackett G, Hepler PK (1996) Tip-localized calcium entry fluctuates during pollen tube growth. Develop Biol **174**: 160-173 PMID: 8626016

Sze H, Liang F, Hwang I (2000) Diversity and regulation of plant Ca^{2+} pumps: Insights from Expression in Yeast. Annu Rev Plant Physiol Plant Mol Biol **51**: 433-62 PMID: 11543429

Twell D, Yamaguchi J, Wing RA, Ushiba J, Mccormick S (1991) Promotor analysis of genes that are coordinately expressed during pollen development reveals pollen-specific enhancer sequences and shared regulatory elements. Genes Dev **5:** 496-507 PMID: 1840556

Watahiki MK, Trewavas AJ, Parton RM (2004) Fluctuations in the pollen tube tip-focused calcium gradient are not reflected in nuclear calcium level: A comparative analysis using recombinant yellow cameleon calcium reporter. Sex Plant Repro **17**: 125-130

Figure legends

Figure 1. Irregular and regular $[Ca^{2+}]_{cyt}$ oscillations observed in elongated *Arabidopsis* pollen tubes 5 h after dissemination under the *in vitro* condition.

A. ECFP, Venus, and Ratio (Venus/ECFP) images of an elongated pollen tube 5 h after dissemination. A tip-focused $[Ca^{2+}]_{cyt}$ gradient was observed. The ratio (Venus/ECFP) in a tip area with a diameter of 6 μm was measured. Bar represents 10 μm.

B. The ratio change in the tip region and the elongation of a normally growing pollen tube. Primarily irregular oscillations were observed, although relatively regular oscillations also were identified in the range marked with a blue line.

C. The ratio change in the tip region of a relatively slowly growing pollen tube (blue line) and the distance moved during monitoring. Regular $[Ca^{2+}]_{cyt}$ oscillations with a large amplitude were observed.

D. Regular oscillations followed by irregular oscillations. Regular oscillations were detected in a stopped or slowly growing pollen tube, whereas irregular oscillations were observed in a growing pollen tube.

Figure 2. Titration curves for YC3.60 and YC4.60.

Figure 3. Irregular oscillations observed in *Arabidopsis* pollen tubes growing through a papilla cell wall (*in vivo* condition) and in pollen tubes growing through a style and then on germination medium (semi-*in vivo* condition).

A. A ratio image of a pollen tube growing though a papilla cell obtained approximately 7.5 min after penetration. A tip-focused $[Ca^{2+}]$ gradient was observed. The papilla cell is marked with a white line.

B. The ratio change in the tip of the pollen tube shown in (A) and the elongation of a pollen tube 5 min after penetration. The amplitude and period of the oscillations were

irregular.

C. Ratio images of a pollen tube that has just passed through the style.

D. The ratio change in the tip of the pollen tube shown in (C) and elongation during monitoring. The amplitude and periodicity of the oscillations were irregular.

Figure 4. The YC3.60 spectrum in the presence of ionophore (A) or in the presence of ionophore and EGTA (B).

Figure 5. The effects of inhibitors on *Arabidopsis* pollen tube elongation.

Figure 6. The effects of inhibitors on the changes in the $[Ca^{2+}]_{cyt}$ in the tip region of *Arabidopsis* pollen tubes growing in the semi-*in vivo* condition.

A. Ratio images of a pollen tube. The numbers in each figure correspond to each point in the graph shown in B. After the addition of CPA, the $[Ca2+]_{cyt}$ increased in a large area containing the tip region (white line).

B. The ratio change in the tip region, an area from the pollen tube shown in (A) with a diameter of 6 μm. Blue line indicates distance from origin. Before the addition of CPA, irregular fluctuations were observed. Two minutes after the addition of CPA (shown with a green arrow), regular oscillations were induced. These oscillations were inhibited by the addition of Gd^{3+} (shown with a green arrow). Red arrows (1) - (5) correlate to the ratio images in Figure 6A.

Figure 7. The effects of Gd^{3+} on the changes in the $[Ca^{2+}]_{cyt}$ in the tip region of *Arabidopsis* pollen tubes growing in the semi-*in vivo* condition.

A. Ratio images of a pollen tube before and after the addition of Gd^{3+}. Numbers in each figure correspond to each point in the graph shown in B. After the addition of Gd^{3+}, the

tip-focused $[Ca^{2+}]_{cyt}$ gradient disappeared and the tip region burst (a white arrow in 3).

B. The ratio change in the tip region before and after the addition of Gd^{3+} (a green arrow) and the elongation of the pollen tube. Red arrows (1) - (3) correlate to the ratio images in Figure 7A. Blue line indicates distance from origin.

Figure 8. Imaging of the $[Ca^{2+}]_{ER}$ in *Arabidopsis* pollen tubes growing in the semi-*in vivo* condition. The YFP image shows the ER, which was localized throughout the pollen tube. In the ratio (Venus/ECFP) images of the ER, high concentration areas were scattered throughout the pollen tube.

Figure 9. The effect of CPA on the $[Ca^{2+}]_{ER}$ in *Arabidopsis* pollen tubes growing in the semi-*in vivo* condition.

A. Ratio images of the ER. The numbers in each figure correspond to each point in the graph shown in B.

B. The ratio change in the tip region. After the addition of CPA, the ratio gradually decreased. After the addition of more CPA, the ratio decreased further.

Figure 10. Regular and irregular $[Ca^{2+}]_{cyt}$ oscillations observed in elongated *N. tabacum* pollen tubes 5 h after dissemination under the *in vitro* condition.

A. ECFP, Venus, and Ratio (Venus/ECFP) images of an elongated pollen tube 5 h after dissemination. A tip-focused $[Ca^{2+}]_{cyt}$ gradient was observed. The ratio was measured in a tip area with a diameter of 8 μm. Bar represents 10 μm.

B. The ratio change in the tip region and elongation during monitoring of a normally growing pollen tube. Regular oscillations were observed but the amplitude was small.

C. The ratio change in the tip region of a normally growing pollen tube and the distance moved during monitoring. The amplitude and periodicity of the oscillations were

irregular.

D. Regular oscillations in a pollen tube that was not growing. The amplitude was larger than that in (A).

Figure 11. Irregular oscillations observed in *N. tabacum* pollen tubes growing on the stigma (*in vivo* condition) and in pollen tubes growing through a style and then on germination medium (semi-*in vivo* condition).

A. The ratio change in the tip and elongation of a pollen tube growing on a stigma. The amplitude and periodicity of the oscillations were irregular, whereas the growth rate was relatively low.

B. The ratio change in growing pollen tubes under the semi-*in vivo* condition. The amplitude and periodicity were irregular.

Supplementary videos

Supplementary Video 1. Irregular $[Ca^{2+}]_{cyt}$ oscillations in a normally growing *Arabidopsis* pollen tube under the *in vitro* condition.

Supplementary video 2. Regular $[Ca^{2+}]_{cyt}$ oscillations in a slowly growing *Arabidopsis* pollen tube under the *in vitro* condition.

Supplementary video 3. Regular oscillations followed by irregular oscillations in an elongated *Arabidopsis* pollen tube under the *in vitro* condition.

Supplementary video 4. Irregular oscillations observed in an *Arabidopsis* pollen tube growing through a papilla cell wall (*in vivo* condition).

Supplementary video 5. Irregular oscillations observed in an *Arabidopsis* pollen tube growing through a style and then on germination medium (semi-*in vivo* condition).

Supplementary video 6. The effects of CPA and Gd^{3+} on the changes in the $[Ca^{2+}]_{cyt}$ in the tip region of *Arabidopsis* pollen tubes growing in the semi-*in vivo* condition.

Supplementary video 7. The effects of Gd^{3+} on the changes in the $[Ca^{2+}]_{cyt}$ in the tip region of an *Arabidopsis* pollen tube growing in the semi-*in vivo* condition.

Supplementary video 8. Imaging of the $[Ca^{2+}]_{ER}$ in an *Arabidopsis* pollen tube growing in the semi-*in vivo* condition.

Supplementary video 9. Regular $[Ca^{2+}]_{cyt}$ oscillations observed in an elongated *N. tabacum* pollen tube.

Supplementary video10. Irregular $[Ca^{2+}]_{cyt}$ oscillations observed in an elongated *N. tabacum* pollen tube.

Supplementary video11. Regular $[Ca^{2+}]_{cyt}$ oscillations observed in a stopping *N. tabacum* pollen tube.

Supplementary video12. Irregular oscillations observed in a *N. tabacum* pollen tube growing on the stigma (*in vivo* condition).

Supplementary video13. Irregular oscillations observed in a *N. tabacum* pollen tube growing through a style and then on germination medium (semi-*in vivo* condition).

Table 1. $[Ca^{2+}]$ oscillation and growth rate of the pollen tube in *Arabidopsis* and *Nicotiana tabacum*

Condition	Growth rate (μm/min)	Max/Min ratio	Amplitude range (μM)	$[Ca^{2+}]_{cyt}$	Exp. No.
Arabidopsis					
in vitro	2.0 ± 1.8	4.5 ± 0.2 / 3.9 ± 0.3	0.3 ± 0.2	0.3 – 0.4	45
in vitro	< 1.0	7.2 ± 0.5 / 3.5 ± 0.2	1.8 ± 0.3	0.3 – 1.0	5
in vivo	3.6 ± 0.5	4.0 ± 0.4 / 3.4 ± 0.3	0.4 ± 0.3	0.3 – 0.4	10
semi-*in vivo*	3.1 ± 0.8	5.1 ± 0.5 / 4.5 ± 0.5	0.3 ± 0.2	0.4 – 0.5	48
Nicotiana tabacum					
in vitro	2.8 ± 1.6	3.9 ± 0.2 / 3.5 ± 0.2	0.2 ± 0.1	0.3 – 0.4	17
in vitro	< 1.0	4.8 ± 0.4 / 2.8 ± 0.2	1.0 ± 0.1	0.1 – 0.5	5
in vivo	0.2 ± 0.1	3.5 ± 0.2 / 3.3 ± 0.1	0.1 ± 0.1	0.3	15
semi-*in vivo*	1.2 ± 0.2	3.9 ± 0.4 / 3.4 ± 0.4	0.3 ± 0.2	0.3 – 0.4	30

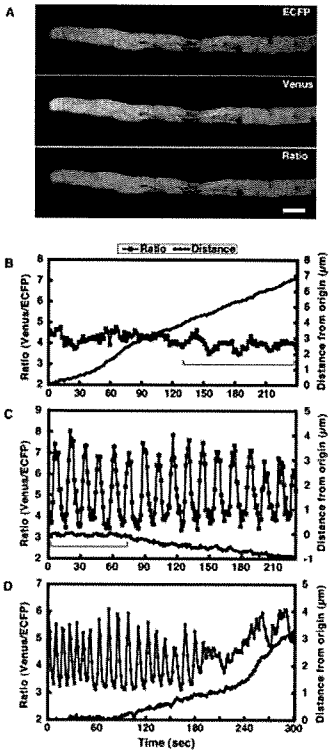

Figure 1. Irregular and regular $[Ca^{2+}]_{cyt}$ oscillations in the elongated *Arabidopsis* pollen tubes 5 hr after dissemination under the *in vitro* condition.

A. ECFP, Venus and Ratio (Venus/ECFP) images. A tip-focused $[Ca^{2+}]_{cyt}$ gradient was observed. The ratio in the tip area with a diameter of 6 μm was measured. Bar represents 10 μm.

B. The ratio change and the elongation of a normally growing pollen tube. Primarily irregular oscillation were observed, although relatively regular oscillations also were in the range marked with a blue line.

C. The ratio change in a stopped pollen tube (blue line) and the distance during monitoring. Regular $[Ca^{2+}]_{cyt}$ oscillation with a large amplitude were observed.

D. Regular oscillations followed by an irregular oscillation. Regular oscillations were detected in a stopped or slowly growing pollen tube, whereas irregular oscillations were observed in a growing pollen tube.

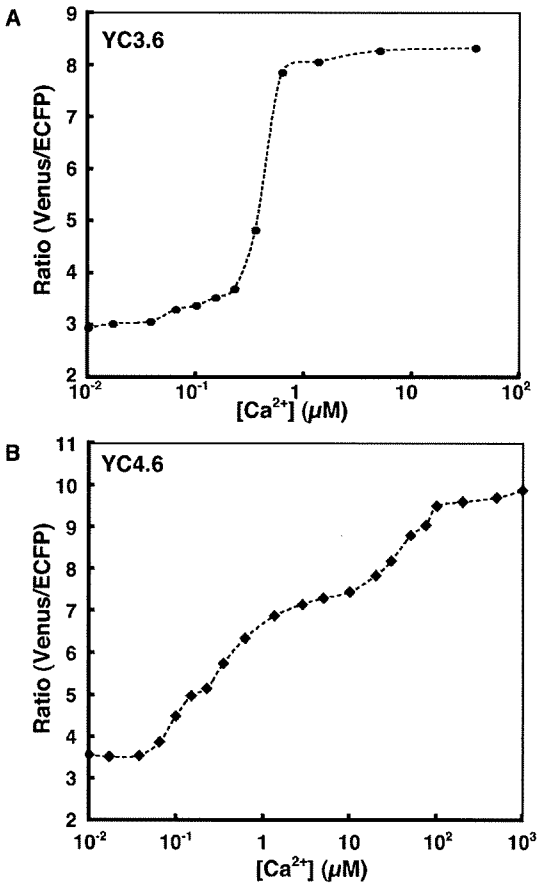

Figure 2. Titration curves for YC3.60 (A) and YC4.60 (B).

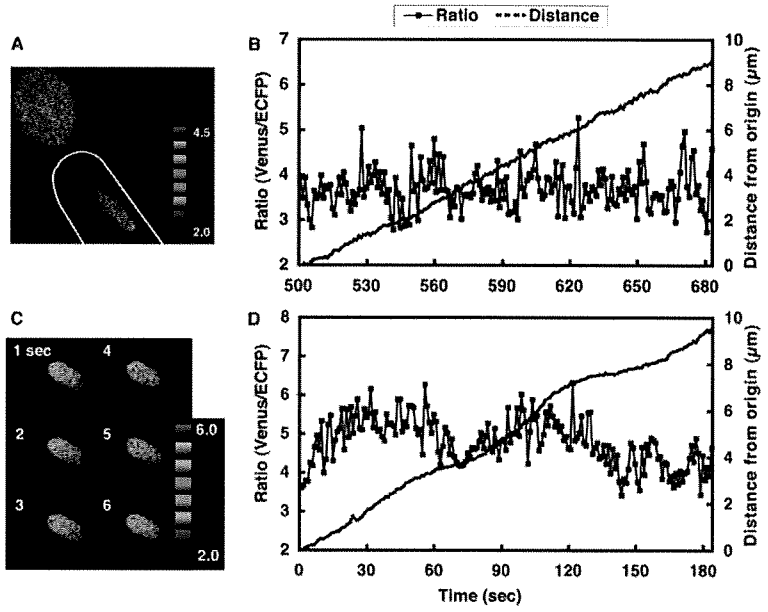

Figure 3. Irregular oscillations observed in *Arabidopsis* pollen tubes growing through a papilla cell wall (the *in vivo* condition) and in pollen tubes growing through a style and then on germination medium (the semi-*in vivo* condition).

A. A ratio image of a pollen tube growing through a papilla cell obtained approximately 7.5 min after penetration. A tip focused $[Ca^{2+}]$ gradient was observed. The papilla cell is marked with a white line.

B. The ratio change in the tip of the pollen tube shown in (A) and the elongation of a pollen tube 5 min after penetration. The amplitude and periodicity of the oscillations were irregular.

C. Ratio images of a pollen tube that has just passed through the style.

D. The ratio change in the tip of the pollen tube shown in (C) and elongation during monitoring. The amplitude and period of the oscillations were irregular.

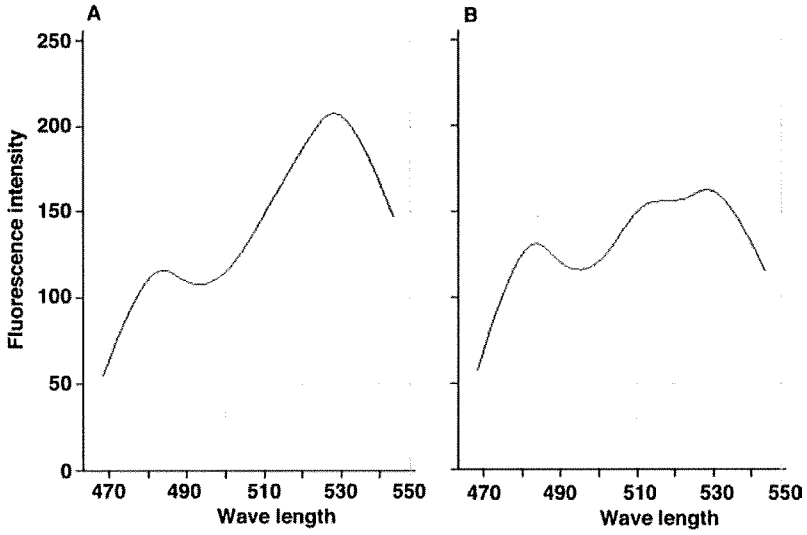

Figure 4. The YC3.60 spectrum in the presence of ionophore (A) or in the presence of ionophore and EGTA (B).

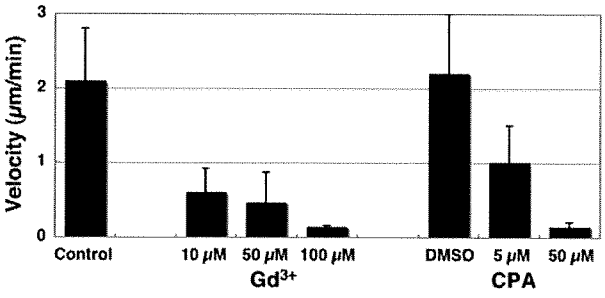

Figure 5. The effects of inhibitors on *Arabidopsis* pollen tube elongation.

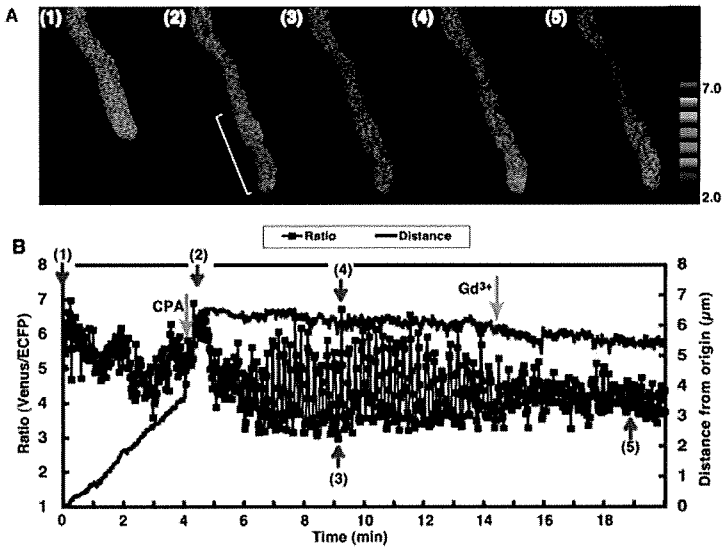

Figure 6. The effects of inhibitors on the changes in the $[Ca^{2+}]_{cyt}$ in the tip region of *Arabidopsis* pollen tubes growing in the semi-*in vivo* condition.

A. Ratio images of a pollen tube. The numbers in each figure correspond to each point in the graph shown in B. After the addition of CPA, the $[Ca^{2+}]_{cyt}$ increased in a large area containg the tip region (a white line).

B. The ratio change in the tip region, an area from the polen tube shown in (A) with a diameter of 6 μm and the elongation of the pollen tube. Blue line indicates the distance to the origin. Before the addition of CPA, irregular oscillations were observed. Two minutes after the addition of CPA (shown with a green arrow), regular oscillations were induced. These oscillations were inhibited by the addition of Gd^{3+}(shown with a green arrow). Red arrows (1) - (3) correlate to the ratio images in Figur 6A.

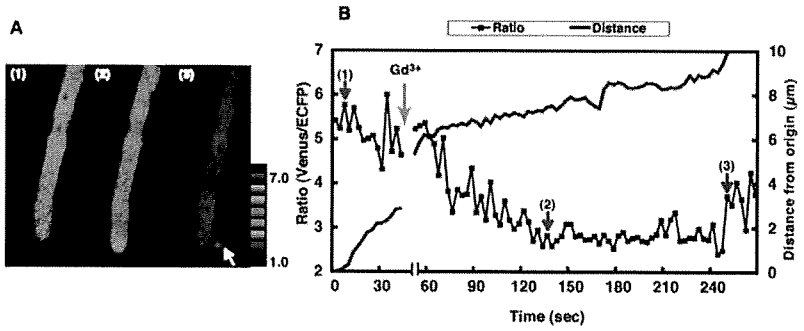

Figure 7. The effects of Gd^{3+} on the changes in the $[Ca^{2+}]_{cyt}$ in the tip region of *Arabidopsis* pollen tubes growing in the semi-*in vivo* condition.

A. Ratio images of a pollen tube before and after the addition of Gd^{3+}. Numbers in each figure correspond to each point in the graph shown in B. After the addition of Gd^{3+}, the tip-focused $[Ca^{2+}]_{cyt}$ gradient disappeared and the tip region burst (a white arrow in 3).

B. The ratio change in the tip region before and after the addition of Gd^{3+} (a green arrow) and the elongation of the pollen tube. Red arrows (1) - (3) correlate to the ratio images in Figure 7A. Blue line indicates the distance to the origin.

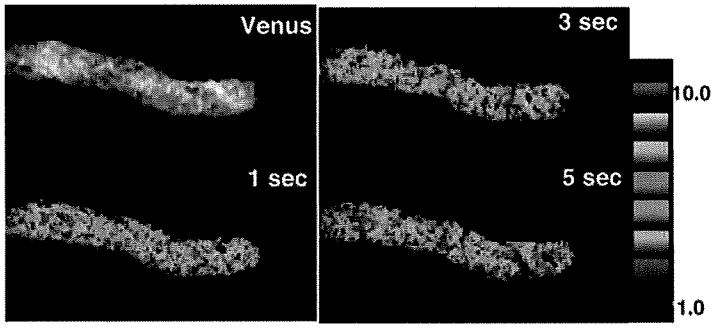

Figure 8. Imaging of the $[Ca^{2+}]_{ER}$ in *Arabidopsis* pollen tubes growing in the semi-*in vivo* condition.

The Venus image shows the ER, which was localized throughout the pollen tube. In the ratio images of the ER, high concentration areas were scattered throughout the pollen tube.

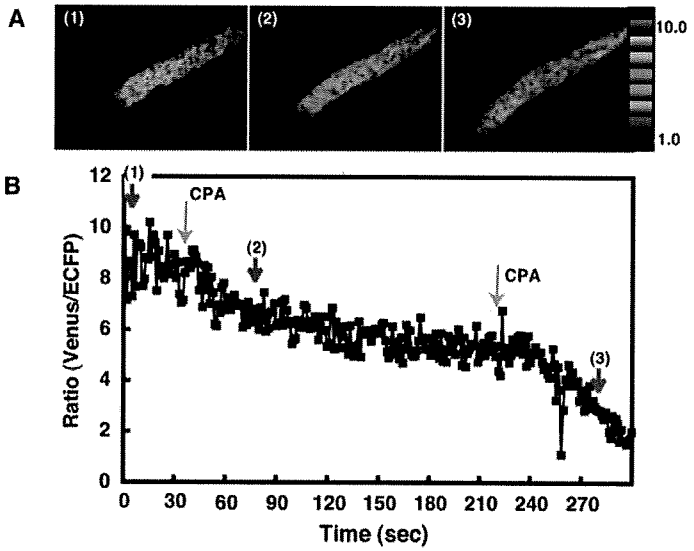

Figure 9. The effect of CPA on the $[Ca^{2+}]_{ER}$ in *Arabidopsis* pollen tubes growing in the semi-*in vivo* condition.

A. Ratio images of the ER. The numbers in each figure correspond to each point in the graph shown in B.

B. The ratio change in the tip region. After the addition of CPA (shown with a green arrow), ratio gradually decreased. After the addition of more CPA(shown with a green arrow) the ratio decreased further. (1), (2) and (3) pointed with red arrows correlate to the ratio images in Figur 9A.

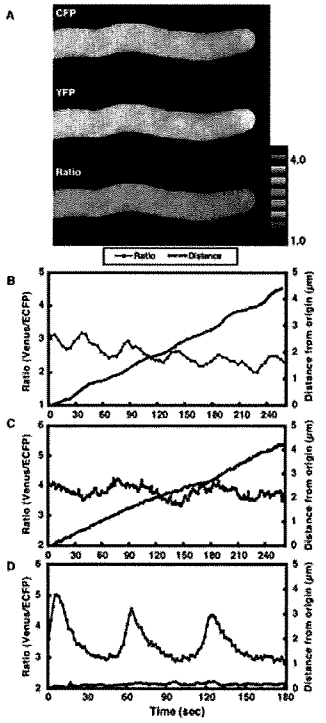

Figure 10. Rregular and irregular $[Ca^{2+}]_{cyt}$ oscillations observed in the elongated *N. tabacum* pollen tubes 5 hr after dissemination under the *in vitro* condition.

A. ECFP, Venus and Ratio (Venus/ECFP) images of an elongated pollen tube 5 hr after dissemination. A tip-focused $[Ca^{2+}]_{cyt}$ gradient was observed. The ratio was measured in a tip area with a diameter of 8 μm . Bar represents 10 μm.

B. The ratio change in the tip region and elongation during monitoring of a normally growing pollen tube. Regular oscillations were observed but the amplitude was small.

C. The ratio change in the tip region of a normally growing pollen tube and the distance moved during monitoring. The amplitude and the periodicity of the oscillations were irregular.

D. Regular oscillations in a pollen tube that was not growing. The amplitude was larger than that in (A).

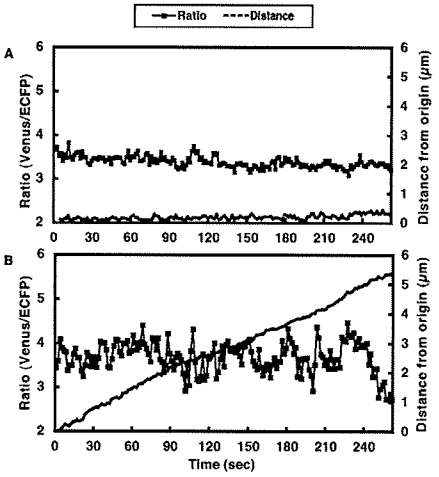

Figure 11. Irregular oscillations observed in in *N. tabacum* pollen tubes growing on the stigma (the *in vivo* condition) and in pollen tubes growing through a style and then on germination medium (the semi-*in vivo* condition).

A. The ratio change in the tip and elongation of a pollen tube growing on a stigma. The amplitude and periodicity of the oscillations were irregular, whereas the growth rate was relatively low.

B. The ratio change in the growing pollen tubes under the semi-*in vivo* condition. The amplitude and periodicity were irregular.

ARTICLE

ACS chemical biology

Reversible Dimerization of *Aequorea victoria* Fluorescent Proteins Increases the Dynamic Range of FRET-Based Indicators

Ippei Kotera[†,§], Takuya Iwasaki[†,§], Hiromi Imamura[‡], Hiroyuki Noji[‡], and Takeharu Nagai[†,*]

[†]Research Institute for Electronic Science, Hokkaido University, Kita-20 Nishi-10, Kita-ku, Sapporo, Hokkaido 001-0020, Japan and [‡]Institute of Scientific and Industrial Research, Osaka University, 8-1 Mihogaoka, Ibaraki, Osaka 567-0047, Japan. [§]These authors contributed equally to this work.

ABSTRACT Fluorescent protein (FP)-based Förster resonance energy transfer (FRET) technology is useful for development of functional indicators to visualize second messenger molecules and activation of signaling components in living cells. However, the design and construction of the functional indicators require careful optimization of their structure at the atomic level. Therefore, routine procedures for constructing FRET-based indicators currently include the adjustment of the linker length between the FPs and the sensor domain and relative dipole orientation of the FP chromophore. Here we report that, in addition to these techniques, optimization of the dimerization interface of *Aequorea* FPs is essential to achieve the highest possible dynamic range of signal change by FRET-based indicators. We performed spectroscopic analyses of various indicators (cameleon, TN-XL, and ATeam) and their variants. We chose variants containing mutant FPs with different dimerization properties, *i.e.*, no, weak, or enhanced dimerization of the donor or acceptor FP. Our findings revealed that the FPs that dimerized weakly yielded high-performance FRET-based indicators with the greatest dynamic range.

Genetically encoded Förster resonance energy transfer (FRET)-based indicators have become useful tools for biological research. FRET-based detection is one of the few techniques that enables the microscopic and noninvasive visualization of physiological events such as second messenger dynamics and enzyme activity in real time and space. Since the pioneering work of Tsien's group on the Ca^{2+} indicator cameleon (*1*), several FRET-based indicators have been developed, and their use has contributed to our understanding of various biological questions. These indicators are generally composed of a sensor domain that is sandwiched between donor and acceptor fluorescent proteins (FPs), such as calmodulin-M13 fusion domain, which is used for Ca^{2+} sensing in cameleon. Conformational changes of the sensor domain alter both the distance and orientation between the donor and acceptor FPs, which are in turn translated into a change in FRET efficiency that is typically detected by a change in the emission intensity ratio. In practice, however, most FRET-based indicators show only a small difference in the emission ratio upon their conformational change. Therefore, improving the dynamic range of the signal change is important for using these indicators to detect biological events with precision and sensitivity.

FRET efficiency is known to decay as a function of the inverse sixth power of the distance between the donor and acceptor, which is generally within 10 nm (*2*). In addition, the relative orientation of the chromophore's transition dipole moment affects the FRET efficiency; thus, careful design and construction of the indicator, especially of the FPs, in which the chromophore is fixed in a β-can shell (*3*), are required. To im-

*Correspondence author, tnagai@es.hokudai.ac.jp.

Received for review October 24, 2009 and accepted January 4, 2010.

Published online January 4, 2010

10.1021/cb900263z